The Gravity Load Simulator – Re-visited

by

P. Wang[a,b] and G.J. Turvey[a]

[a]**Engineering Department, Lancaster University, Bailrigg, Lancaster, LA1 4YW, UK**

[b]**OneSubsea, a Schlumberger Company, 10 Furness Business Park, Barrow-in-Furness, Cumbria, LA14 2PE, UK**

Abstract

A review of loading arrangements for lateral buckling tests on pultruded glass fibre reinforced polymer (GFRP) beams is presented. It is suggested that the *Gravity Load Simulator* (GLS), used for similar tests on steel beams could also be used for lateral buckling tests on GFRP beams and, moreover, it could be analysed and designed using exact calculations rather than the iterative method used more than 50 years ago. This conclusion is demonstrated by re-analysing the old iteratively designed GLS. The exact analysis is then used to analyse and design a new GLS for lateral buckling tests on pultruded GFRP beams. The new GLS was fabricated from aluminium bar and plate and details of its overall dimensions and layout and the types of bearings used in its pin joints are described. Thereafter, the test arrangement and instrumentation used to demonstrate the GLS's accuracy, i.e. maintaining the horizontal translation of the jack's base as the GLS sways in the lateral buckling plane, is presented. It is shown that the GLS performs extremely well and its use in laboratory testing is illustrated.

Keywords: Beams, Gravity Loading, Lateral Buckling, Load Testing

Introduction

Awareness of the advantages of fibre reinforced polymer (FRP) composites, e.g. low self-weight, durability etc., for infrastructure applications has been increasing amongst the civil and structural engineering community, especially since the advent of code-like design guidance such as [1 – 3]. These circumstances have led to increasing interest in static load testing of FRP structural members (beams, columns etc.) and sub-/full-scale structures in order to determine their stiffness and strength characteristics and demonstrate their compliance with these code-like documents. Although static load testing of steel, aluminium, concrete, and timber structural members has a long history, testing of glass and carbon fibre-reinforced polymer (GFRP) and (CFRP) structural components is much less extensive. In fact, compliance testing of FRP components has been (and in many cases still is) undertaken with modifications to reference standards developed for steel and aluminium materials.

Unlike in aerospace, GFRP composites tend to dominate in infrastructure applications, because CFRP composites are much more expensive. Moreover, compliance for flexural design of GFRP composites requires satisfaction of serviceability rather than ultimate limit state criteria, i.e. deflections must not become excessive or buckling must not arise before the ultimate limit state of collapse is reached. In consequence, there has been considerable research on modelling the deformation and buckling behaviour of beams and columns taking account of the anisotropic nature of these materials. By contrast, the quantity of complementary test work, particularly for lateral buckling of GFRP beams, is small. This is largely due to the difficulty of ensuring that the load maintains its gravitational orientation as the beam cross-section transitions from a vertical displacement state to a combined vertical, horizontal and rotational displacement state. Nevertheless, a number of lateral buckling tests on three-point flexure of single-span GFRP beams and tip-loaded GFRP cantilevers have been reported [4 – 13] and will now be briefly reviewed.

Amongst the earliest lateral buckling tests are those described in [4] and [5] on 1.5 m span pultruded GFRP I-section beams subjected to a vertical point load at mid-span. The simply supported ends of the beams were stabilised to prevent lateral deflection, lateral bending, warping and twisting. A transverse slider on top of a steel ball joint transmitted the load from the upper platten of the test machine to the beam's top flange. This

system allowed the beam to translate laterally as well as rotate. The buckling load was considered to correspond to the value recorded by the test machine when the lateral displacement was 2 mm.

Amongst the earliest cantilever lateral buckling tests on rectangular- and I-section pultruded GFRP beams are those reported in [6] and [7]. Figure 1 shows a rectangular-section cantilever buckled laterally by a tip load acting at the mid-depth of the free end [6]. The connection between the load hanger and the cantilever's free end is a lightweight diamond-shaped self-equilibrating structure. The horizontal steel compression rod preserves the tensile steel wire's diamond shape, so that end of the cantilever may rotate unhindered. A protractor attached to the end of the cantilever together with a theodolite (aligned with the unloaded axis of the cantilever) recorded the end rotation and horizontal translation. In [7] a modified version of the load arrangement was used in lateral buckling tests with the load at different heights above/below the mid-depth of the end cross-section. Other researchers (see [8] – [11]) have used variations of the aforementioned loading arrangements to carry out similar lateral buckling tests on mid-span point loaded simply supported I-section beams and tip loaded I- and channel-section cantilevers. In the channel-section cantilever tests a simple slider attached to the free end was used to position the load at the shear centre of the cross-section.
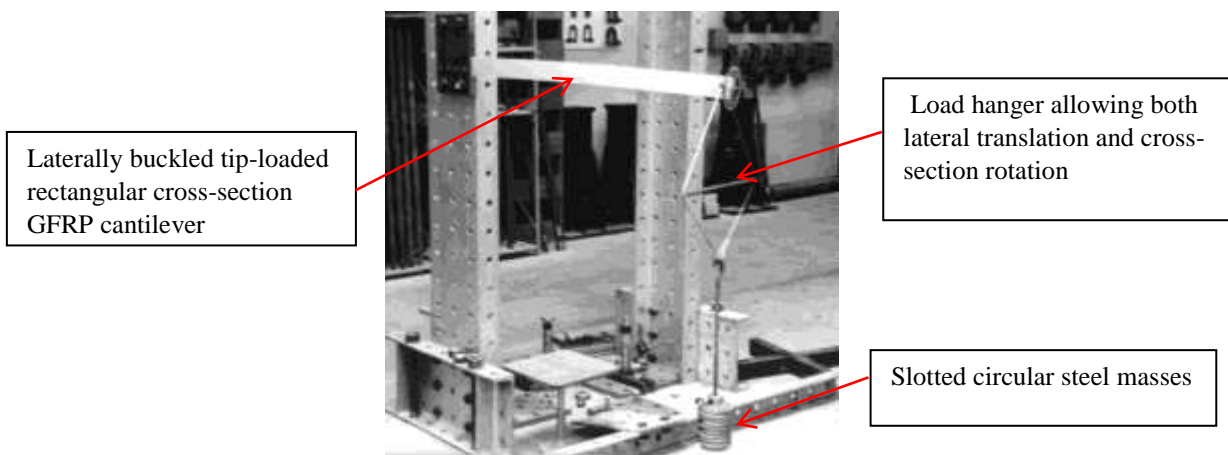

Figure 1: Lateral buckling tests on a tip-loaded pultruded GFRP cantilever beams.

A more sophisticated setup for conducting lateral buckling tests on one size of I-section and three sizes of channel-section GFRP beams with two sets of end conditions and a vertical point load applied at mid-span is presented in [12] and [13]. The setup uses two pulley wheels connected by a wire loop. The load hanger is supported from the smaller lower pulley and the beams pass through a rectangular cut-out in the larger pulley wheel, so that their centroidal axes or shear centres coincide with the pulley's axis of rotation.

Another system, which was investigated some time ago by the second Author, involves supporting the jack load on an air-bearing, so that it may follow the beam without imposing any restraints as its cross-section undergoes vertical, horizontal and rotational displacements (see Figure 2). This system has the advantage that it can maintain the load's verticality in the presence of horizontal and rotational displacements even when the local plane of flexure and rotation is not normal to the beam's initial plane of flexure. Hence, the system is able to function when the load is applied anywhere along the length of the beam. Nevertheless, supporting the jack load on an air-bearing has its limitations. The setup, shown in Figure 2, only allows the jack to apply a vertical compressive load. If a tensile vertical load is required, a modified base plate has to be used, i.e. the pressurised air has to act on the upper surface of the jack's baseplate and this requires a cover plate with a central circular hole to accommodate the jack. The air pressure is reacted by the outer part of the plate. Furthermore, the size of the hole limits the jack's horizontal movement, which is usually less than that of the compressive loading arrangement. A potentially more serious shortcoming with the air-bearing setup is that, for very high pressures, the cushion of air supporting the jack can become unstable, i.e. the pressurised air does not exit uniformly around the edge of the jack's baseplate. The consequence is that the jack vibrates and applies a fluctuating rather than a static load to the beam. The system shown in Figure 2 was explored some years ago in the Engineering Department to carry out lateral buckling tests on GFRP cantilever beams. However, it was abandoned in favour of an alternative loading system – the *Gravity Load Simulator* (GLS) – developed by Yarimci et al. [14] more than half a century ago.
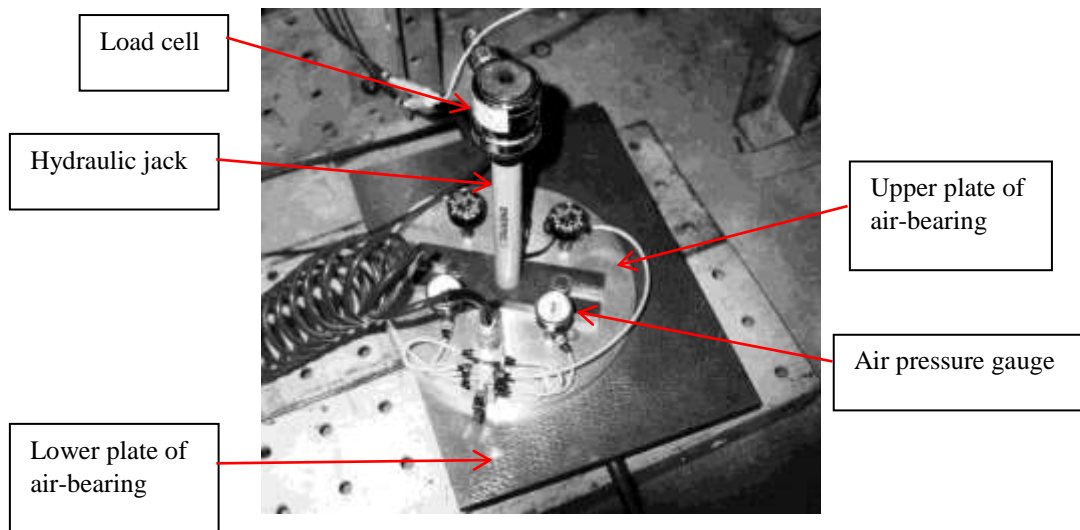
Figure 2: Jack supported on an air bearing

The GLS is based on Robert's three-bar mechanism (see Figure 3) which allows the lowest apex of an inverted rigid isosceles triangle to follow a fixed-height horizontal path as the mechanism moves to the right (or left) in the sway plane. By attaching the jack to the lowest apex of the triangle, the system enables the beam to be subjected to gravitational (vertical) loading as its cross-section translates and rotates in the same plane. As with any loading mechanism, there are limitations (drawbacks) with the GLS. The size of the sway is limited by the size of the mechanism and the members of the mechanism have to be designed to support the required maximum jack load. Furthermore, as discussed later, the jack attached to the mechanism is only truly vertical in the initial symmetric (no side-sway) configuration and at the designed half-sway limits. Furthermore, the jack's base deviates from the truly horizontal as the mechanism sways. However, in both instances, these deviations are very small, as demonstrated later.
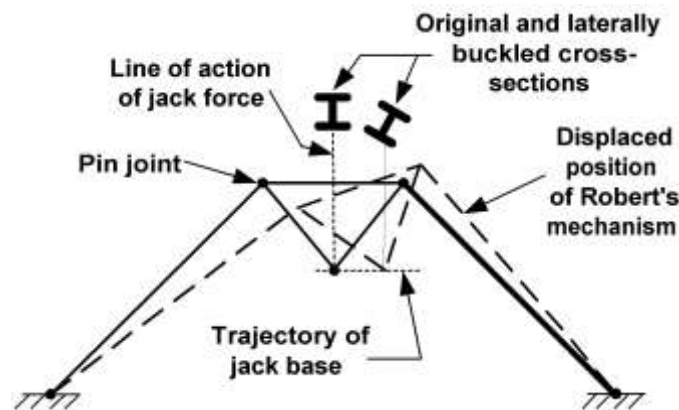

Figure 3: Schematic diagram of the sway translation of the GLS – based on Robert's three-bar mechanism

The design analysis of the sway mechanism presented by Yarimci et al. in [14] uses an iterative procedure to define each position of the mechanism as the jack load translates horizontally with the beam. In consequence, the possibility of using a simple closed-form analysis has been over-looked. Recently, the Authors have developed a closed-form exact analysis of the GLS mechanism. The subsequent sections of the paper describe the analysis and present comparisons with the design presented in [14]. They also tabulate general formulae for the forces in the members of the mechanism as it sways (see Figure 3). In addition, details are provided of the analysis and design of an aluminium GLS, which has been tested to determine how well it performs in practice. Finally, its use in conducting lateral buckling tests on a pultruded GFRP WF beam is illustrated.

Exact Analysis of the GLS

3

Calculation of the GLS's sway co-ordinates

In any experimental setup involving the use of a GLS to apply loads to a beam, the *initial* configuration of the GLS is symmetric with the vertical jack load aligned with its axis of symmetry (see Figure 4).

For the purposes of the analysis, it is convenient to locate the origin of co-ordinates x, y at the pin joint A. The other three pin joints are located at B, C and D. The trapezoidal shape CZDYX represents a rigid area (plate or frame) connected to the GLS at the hinges C and D. The base of the vertical jack is pinned to the vertical axis of symmetry of the rigid shape at E.

The principal dimensions of the GLS are the lengths L of the two inclined arms AC and BD, the bases of which, A and D, are a distance H apart. The distance between the two upper hinges C and D is r. The other significant dimension is EZ of length d. In [14] d is defined as the *load height*.

The GLS is a one-degree of freedom mechanism, which, for the convenience of analysis and design, may be defined as the x – co-ordinate of the pin joint at C or the angle α between the x-axis and the arm AC, respectively.
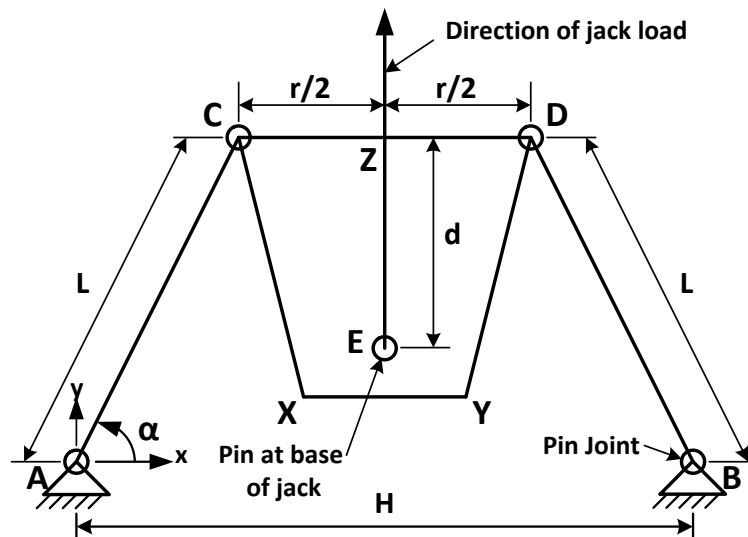

Figure 4: Initial loading set up of a GLS

In order to analyse the in-plane sway of the GLS, it is necessary to define the co-ordinates of the joints for an arbitrary transverse sway position (see Figure 5). In Figure 5 the dashed line extensions of the two arms AC and BD intersect at the point F, which is the centre of rotation. In order for the jack to be able to apply a vertical load to the beam under test it is necessary for its pinned base support at E to be vertically below the centre of rotation at F. In addition, the point E should remain at the same height above the level of the pins at A and B irrespective of the sway translation of the GLS. The extent to which the latter requirement is satisfied is explained after the exact analysis of the mechanism has been presented.
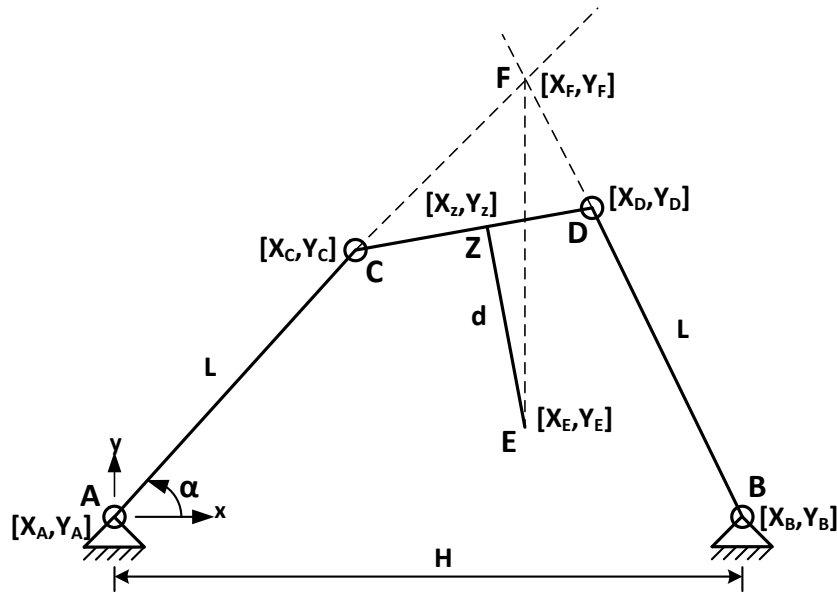
Figure 5: Arbitrary sway position of the GLS (<u>Note</u>: Line EF is inclined at a very small angle θ_{EF} to the vertical)

If it is assumed that x_C is the known single degree of freedom of the GLS, then it remains to establish how the other co-ordinates y_C, x_D, y_D are related to x_C in order to completely determine the sway configuration of the GLS. This is explained as follows, y_C and y_D may be expressed as,

$$y_C = \sqrt{L^2 - x_C^2} \tag{1}$$

$$y_D = \sqrt{L^2 - \left(H - x_D\right)^2} \tag{2}$$

Now, from Eqs. (1) and (2), L^2 may be expressed as,

$$L^2 = x_C^2 + y_C^2 = \left(H - x_D\right)^2 + y_D^2 \tag{3}$$

Furthermore, the square of the length of the line CD is,

$$r^2 = \left(x_D - x_C\right)^2 + \left(y_D - y_C\right)^2 \tag{4}$$

After some manipulation and substitution, the following expression for x_D is obtained as,

$$x_D = \frac{1}{H - x_C}\left(\frac{H^2 + r^2}{2} - x_C^2 + \sqrt{r^2 - \left(x_D - x_C\right)^2}\sqrt{L^2 - x_C^2}\right) \tag{5}$$

In [14] Yarimci et al. did not progress their analysis any further. Instead, they solved Eq.(5) iteratively and in so doing did not identify the exact solution for x_D. However, after some further manipulation and substitution the following alternative equation is obtained:-

$$x_D = \frac{1}{H - x_C}\left[\frac{H^2 + r^2 - 2L^2}{2} + \sqrt{L^2 - x_C^2}\sqrt{L^2 - \left(H - x_D\right)^2}\right] \tag{5a}$$

5

In order to simplify Eq.(5a) it is convenient to introduce the following substitutions,

$$a = H - x_C \tag{6}$$

$$b = \frac{H^2 + r^2 - 2L^2}{2} \tag{7}$$

and
$$c = \sqrt{L^2 - x_C^2} \tag{8}$$

After substituting Eqs.(6) – (8) into Eq.(5a) and squaring, the following quadratic equation for x_D is obtained:-

$$e x_D^2 + f x_D + g = 0 \tag{9}$$

where the coefficients of the variables x_D^2 and x_D are:-

$$e = \left(a^2 + c^2\right) \tag{10}$$

$$f = -2\left(ab + c^2 H\right) \tag{11}$$

$$g = b^2 + c^2\left(H^2 - L^2\right) \tag{12}$$

Hence, the solution for x_D may be defined explicitly as,

$$x_D = \frac{-f + \sqrt{f^2 - 4eg}}{2e} \tag{13}$$

Therefore, once x_C has been defined, x_D can be determined from Eq.(13) and then y_C and y_D may be determined from Eqs.(1) and (2) respectively, so that the spatial position of the GLS becomes fully defined.

Calculation of the co-ordinates $\left(x_F, y_F\right)$ of the instantaneous centre of rotation

The instantaneous centre F with co-ordinates $\left(x_F, y_F\right)$ in Figure 5 is at the intersection of the dashed line extensions of the GLS's arms, AC and BD. The equations of the lines AC and BD are respectively,

$$y = \frac{y_C}{x_C} x \tag{14}$$

and
$$y = \frac{y_D}{x_D - H}\left(x - H\right) \tag{15}$$

Hence, substituting x_F into the right hand sides of Eqs. (14) and (15), and equating and re-arranging them gives the x_F co-ordinate as,

$$x_F = \frac{x_C y_D H}{y_C\left(H - x_D\right) + x_C y_D} \tag{16}$$

and y_F is then obtained from Eq.(14).

Calculation of the load height d

The load height d is determined from the co-ordinates $\left(x_E, y_E \right)$ of the jack's pinned base at E and the equation of the line EZ which is the perpendicular bisector of the top member CD of length r of the GLS.

The slope k_r of the line CD is,

$$k_r = \frac{y_D - y_C}{x_D - x_C} \tag{17}$$

Therefore, as the line EZ is the perpendicular bisector of the line CD its slope k_d is equal to the negative reciprocal of the slope k_r of the line EZ. Furthermore, the perpendicular bisector EZ passes through the mid-point of the line CD. Hence, the equation of the line EZ is,

$$y - \frac{y_C + y_D}{2} = -\frac{x_D - x_C}{y_D - y_C}\left(x - \frac{x_C + x_D}{2} \right) = k_d\left(x - \frac{x_C + x_D}{2} \right) \tag{18}$$

Now as point E lies on this line and is also on the vertical dashed line drawn from the instantaneous centre F, then $x = x_E = x_F$ and $y = y_E$, so that Eq.(18) becomes,

$$y_E = k_d\left(x_F - \frac{x_C + x_D}{2} \right) + \frac{y_C + y_D}{2} \tag{19}$$

Hence, the square of the length EZ, i.e. d^2, is,

$$d^2 = \left(x_F - \frac{x_C + x_D}{2} \right)^2 + \left(y_E - \frac{y_C + y_D}{2} \right)^2 = \left(x_F - \frac{x_C + x_D}{2} \right)^2 \left(1 + k_d^2 \right) = \left(x_F - \frac{x_C + x_D}{2} \right)^2 \left(\frac{r}{y_D - y_C} \right)^2 \tag{20}$$

so that,

$$d = \frac{r}{y_D - y_C}\left(x_F - \frac{x_C + x_D}{2} \right) \tag{21}$$

Calculation of the inclination of the jack load to the vertical

Eq.(21) determines the load height d for the value of x_F, the x co-ordinate of the instantaneous centre, F. The significance of this is that when there is no side sway and the GLS's configuration is symmetrical, as shown in Figure 4, the jack load is vertical. Likewise, when the side sway is equal to $\pm x_F$, the jack's pin joint at E is also directly below the instantaneous centre F, so that the jack is vertical. Only at these specific side-sway positions will the jack be vertical. At all other positions between the symmetrical position and $\pm x_F$ the jack will be slightly out of vertical alignment and, as a result, will apply a small horizontal force to the beam. The magnitude of the horizontal force is determined from the slope of the jack and the jack's load.

The co-ordinates of the jack's pinned base E and the instantaneous centre of rotation F are $\left(x_E, y_E \right)$ and $\left(x_F, y_F \right)$, respectively. Furthermore, E lies on the perpendicular bisector of the GLS's top width CD, i.e. the line of length r. Hence, the equation of the perpendicular bisector is,

$$y_E - \frac{y_C + y_D}{2} = k_d \left(x_E - \frac{x_C + x_D}{2} \right) \tag{22}$$

Now the distance between the base E and the centre of the top width CD is equal to d and d^2 may be expressed as,

$$d^2 = \left(x_E - \frac{x_C + x_D}{2} \right)^2 + \left(y_E - \frac{y_C + y_D}{2} \right)^2 \tag{23}$$

Hence, substituting Eq.(22) into Eq.(23) and taking the square root gives,

$$x_E = \frac{x_C + x_D}{2} + \frac{d}{\sqrt{1 + k_d^2}} \tag{24}$$

and substituting Eq.(24) into Eq.(22) and re-arranging gives,

$$y_E = \frac{y_C + y_D}{2} - \frac{k_d d}{\sqrt{1 + k_d^2}} \tag{25}$$

Therefore, the inclination of the jack load to the vertical is,

$$\theta_{EF} = \frac{x_E - x_F}{y_E - y_F} \tag{26}$$

Checking the displacements of the GLS and the verticality of the jack

In order to carry out these tasks, it is more convenient to change the single degree of freedom x_C, i.e. the x-co-ordinate of the pin joint C, to the angle α subtended by the GLS's arm AC to the horizontal. The following procedure may be adopted.

1. Choose the basic dimensions of the GLS, i.e. the lengths H, L and r.

2. Hence, evaluate the co-ordinates (x_C, y_C) and (x_D, y_D) of the pin joints C and D for the initial symmetrical configuration of the GLS.

3. Then evaluate the initial value of the angle α for the initial configuration, i.e. $\alpha = \alpha_0$, as follows,

$$\alpha_0 = \cos^{-1} \left(\frac{H - r}{2L} \right) \tag{27}$$

4. Hence, evaluate the GLS's minimum angle $\alpha_{\min}$, i.e. when the left hand arm AC and the top width CD are collinear and the GLS defines a triangle with vertices at A, D and B. In this situation, the slopes of AC and CD are equal so that

$$\frac{y_C}{x_C} = \frac{y_D}{x_D} \tag{28}$$

5. The initial angle α_0 may then be reduced successively by n small decrements $\delta\alpha$ to α_{min} where,

$$\delta\alpha = \frac{(\alpha_0 - \alpha_{min})}{n} \tag{29}$$

6. Calculate the co-ordinates (x_E, y_E) of the jack's pinned base E and the co-ordinates of the instantaneous centre (x_F, y_F) as the angle α_0 reduces to α_{min} using Eqs.(24) and (25).

7. The vertical angle of the jack's base is then determined from Eq.(26).

Verification of the exact analysis by comparison with Yarimci et al.'s GLS design

As mentioned earlier Yarimci et al. [14] used an iterative procedure to determine the displacements of the pin joints at C and D as the GLS sways. It is, therefore, convenient to re-analyse their mechanism to verify the Authors' exact analysis.

The basic dimensions of Yarimci et al's GLS are given in Table 1.

Table 1

Dimensional and non-dimensional details of Yarimci et al's [14] GLS

GLS Components and Sways	Component and Sway Dimensions [m]	Dimensionless Components and Sways (w.r.t. H)
Base Length (H)	3.3528	1.0000
Arm Length (L)	1.63076	0.4864
Top Width (r)	0.9906	0.2954
Full-Sway (S)	0.4064	0.1212
Half -Sway (S/2)	0.2032	0.0606
Load Height (d)	0.93147	0.27781

In order to verify the exact analysis and compare its performance with Yarimci et al's. iteration-based design, it is convenient to non-dimensionalise these dimensions with respect to the base length H.

The exact analysis has been carried out using the dimensionless values taken from Table 1. According to this analysis for the jack to be truly vertical, i.e. $\theta_{EF} = 0$, the value of the non-dimensional load height is $\frac{d}{H} = 0.27799$. Thus, the exact analysis gives a load height 0.07% lower than Yarimci et al's value.

The exact analysis has been used to evaluate the jack's inclination to the vertical θ_{EF} for both $\frac{d}{H}$ values for a range of the dimensionless side-sways $\frac{x_E}{H} = 0.5 \rightarrow 0.6212$. The two sets of results are shown in Figure 6. It is evident that the Author's results are more accurate than Yarimci et al's results, obtained just over 50 years ago, since the curve of their graph intersects the abscissa at the half-sway point.
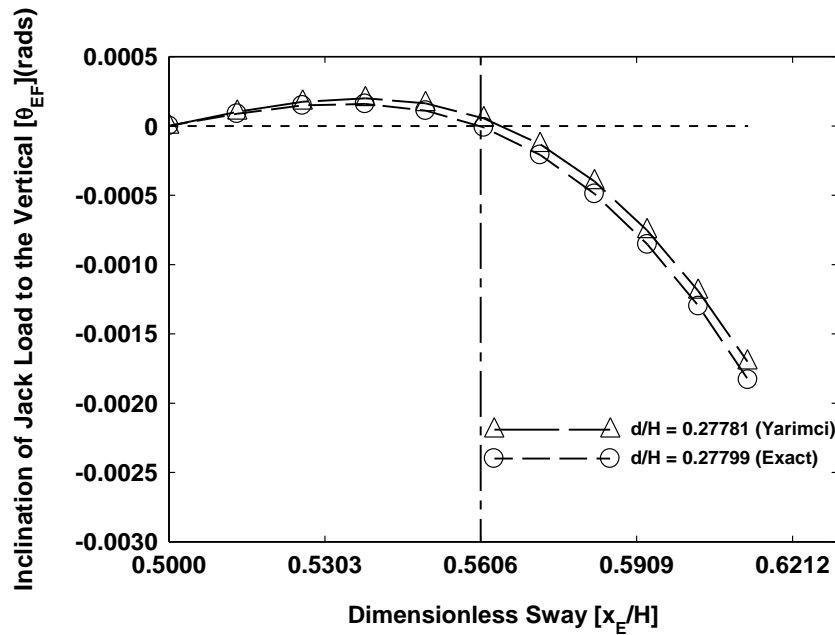
9

Figure 6: Inclination of the jack load to the vertical θ_{EF} versus side-sway $\dfrac{x_E}{H}$

It is also evident from Figure 6 that for side-sway values between the symmetric configuration $\dfrac{x_E}{H} = 0.5$ and the half side-sway value $\dfrac{x_E}{H} = 0.5606$ the jack's inclination θ_{EF} is positive. This implies that a small horizontal load will be applied to the component under test in the direction of sway in addition to the vertical component of the load. The maximum value of this horizontal load component is about 0.02% of the vertical load component. However, when the GLS sways beyond the half-side-sway point, Figure 6 shows that the jack's inclination θ_{EF} changes to negative values. This implies that there is a horizontal load component, which tends to restrain the side-sway. Again, Figure 6 shows that at the full-sway position the horizontal load component amounts to 0.24% of the vertical load component. In most practical situations, this value may be disregarded.

It is also of interest to consider the dimensionless vertical movement of the jack's base, i.e. $\dfrac{y_E}{H}$, as the GLS sways to the full extent. The results of these calculations are shown in Figure 7.
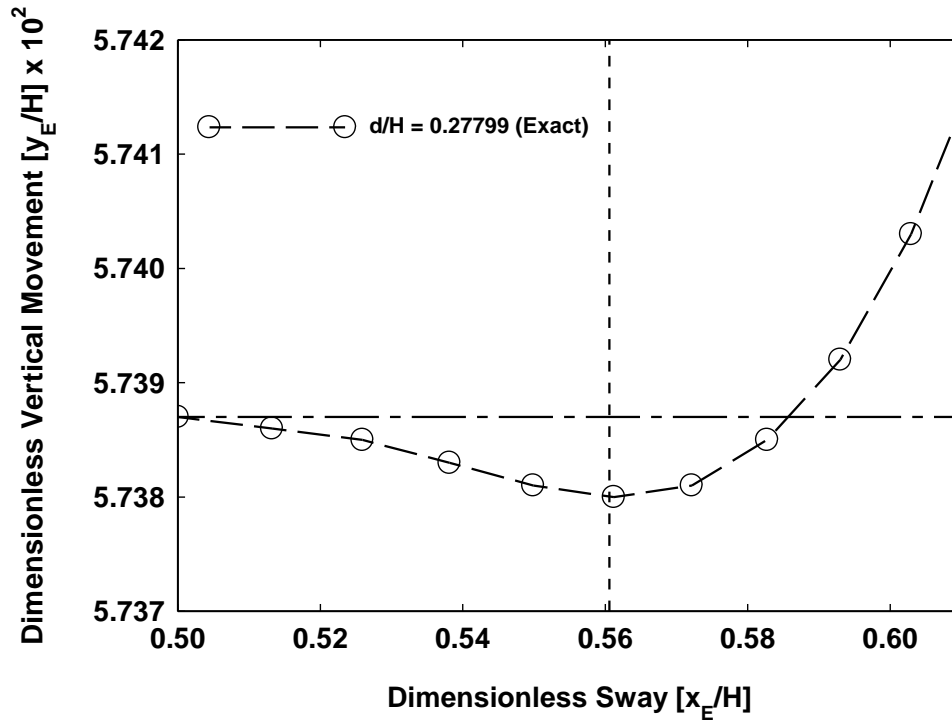
10

Figure 7: Vertical jack movement $\dfrac{y_E}{H}$ versus side-sway $\dfrac{x_E}{H}$

It is evident that for most of the dimensionless sway range, i.e. $\dfrac{x_E}{H} = 0.5 \to 0.58$, the dimensionless vertical movement of the jack's base, i.e. $\dfrac{y_E}{H} \leq 0.00001$, which indicates that the base can be considered to be moving along a horizontal line.

The aforementioned results in Figures 6 and 7 demonstrate that within the half-sway range the GLS is able to provide a very accurate simulation of true gravity loading on any structure or component to which it is connected.

Calculation of the loads in the members of the GLS

Once the geometry of the GLS is determined, the magnitudes of the internal forces in its members may be calculated. Figure 8 represents an arbitrary sway position of the GLS with its members labelled 1 – 5.
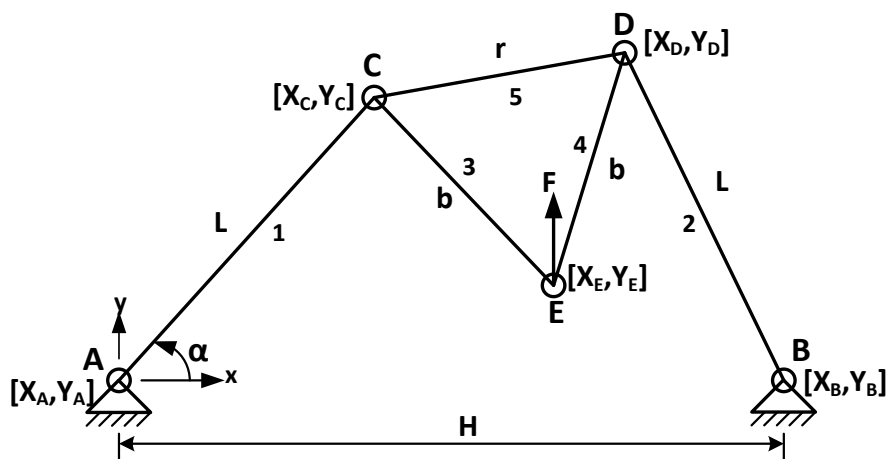
Figure 8: Diagram showing the member numbers and lengths of the GLS for an arbitrary sway angle α

Assuming that the vertical jack load at the joint E is F and the forces in the members are $F_i (i = 1 - 5)$ and their corresponding orientations to the horizontal are $\theta_i (i = 1 - 5)$, equilibrium equations may be set up for each of the joints E, C and D to determine the values of F_i and θ_i. The relevant equations for these quantities are given in Table 2.

Table 2

Equations for the member forces and their orientations at joints E, C and D

of the GLS

Pin Joint	Mechanism's Member Forces in Terms of the Vertical Jack Force F at Joint E	Inclinations of the Member Forces to the Horizontal
E	$F_3 = \dfrac{F \cos\theta_4}{\cos\theta_3 \sin\theta_4 + \sin\theta_3 \cos\theta_4}$ $F_4 = \dfrac{F_3 \cos\theta_3}{\cos\theta_4}$	$\tan\theta_3 = \dfrac{y_C - y_E}{x_E - x_C}$ $\tan\theta_4 = \dfrac{y_D - y_E}{x_D - x_E}$
C	$F_1 = \dfrac{F_5 \cos\theta_5 + F_3 \cos\theta_3}{\cos\theta_1}$ $F_5 = F_3 \dfrac{\sin\theta_3 \cos\theta_1 + \cos\theta_3 \sin\theta_1}{\sin\theta_5 \cos\theta_1 - \cos\theta_5 \sin\theta_1}$	$\tan\theta_1 = \dfrac{y_C}{x_C}$ $\tan\theta_5 = \dfrac{y_D - y_C}{x_D - x_C}$
D	$F_2 = \dfrac{F_4 \cos\theta_4 + F_5 \cos\theta_5}{\cos\theta_5}$	$\tan\theta_3 = \dfrac{y_D}{H - x_D}$

As already mentioned, the GLS is a single-degree of freedom system in terms of the angle α (see Figure 8). Based on the dimensions of Yarimci's GLS (see Table 1) in its initial symmetric position $\alpha = \alpha_0 = 43.6^o$. The maximum sway of the GLS corresponds to collinearity of the members AC and CD for the sway direction to the right, shown in Figure 8. In this position $\alpha = 28.5^o$.

If it is assumed that the jack force $F = 1$, then the forces in the GLS's pin-jointed members may be evaluated using the equations in Table 2. The variation of the member forces is shown in Figure 9 for an angular range of about 8°.
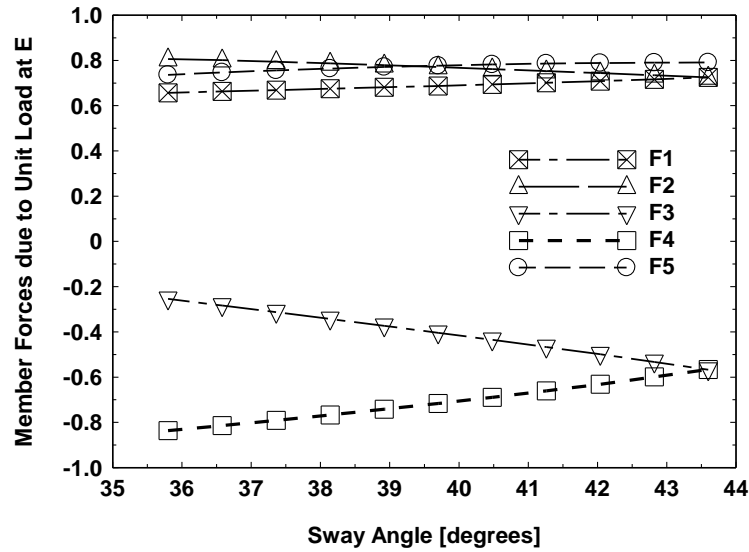
Figure 9: Forces in the GLS's members versus sway angle α

A new optimally designed GLS

As is clear from Figure 4, there are three dimensions of the GLS that have to be determined before the structural aspects of the design may be progressed. They are the base width H the arm lengths L and the top width r. The base width H was determined by the spacing of the holding down bolts on the strong floor of the test laboratory. It was decided to set $H = 1219.2\,mm$ – a length equal to three times the bolt spacing. In order to allow the simulator to accommodate the anticipated lateral deformation of the beam(s) to be tested, it was decided to fix the arm lengths equal to $0.5H = 609.6\,mm$. The maximum side-sway, based on previous lateral buckling tests on tip-loaded cantilevers, was determined as $150\,mm$, so that the half side-sway dimension is $75\,mm$. The third principal dimension, viz. the top width r, is less easy to define precisely. Therefore, it was decided to explore its effect on the functioning of the GLS; in particular its ability to ensure zero slope at the half side-sway position and to minimise the inclination of the jack load to the vertical θ_{EF} over the half side-sway range. Consequently, the GLS's sway performance was determined by incrementing the dimensionless top width $\dfrac{r}{H}$ from 0.2 to 0.4 in steps of 0.02 and determining the corresponding changes in the dimensionless load height $\dfrac{d}{H}$. The results of these calculations are shown in Table 3.

13

Table 3

Effect of top width on load height

Dimensionless Top Width $\bar{r} = \dfrac{r}{H}$	Dimensionless Load Height $\bar{d} = \dfrac{d}{H}$
0.20	0.1864
0.22	0.2010
0.24	0.2168
0.26	0.2341
0.28	0.2530
0.30	0.2739
0.32	0.2972
0.34	0.3234
0.36	0.3528
0.38	0.3862
0.40	0.4240

For the top three pairs of dimensionless top widths and load heights in Table 3 the inclinations of the jack load to the vertical θ_{EF} have been calculated for the dimensionless sway range $\dfrac{x_E}{H}$. These values are plotted in Figure 10. As expected, all three curves intersect the abscissa at the half-sway value, thereby confirming that at this position $\theta_{EF} = 0$ and the jack load is vertical. However, between the no-sway and half-sway locations, the values of θ_{EF} differ significantly, with the smallest values over the half-sway range corresponding to a dimensionless top-width of 0.24. This outcome, suggests that further reductions in the θ_{EF} values over the half-sway range could arise from further refinement of the calculations.
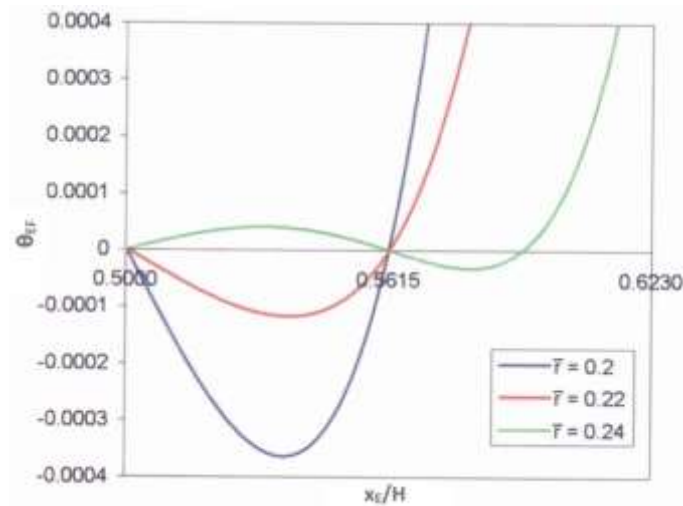

Figure 10: Jack load inclination to the vertical θ_{EF} versus side-sway $\dfrac{x_E}{H}$ for three values of the dimensionless top-width of the GLS

The calculations of the load-slopes over the half side-sway were repeated by incrementing the dimensionless top-widths by 0.002 between 0.22 and 0.24 in order to determine the optimum value of the top-width, i.e. the value giving the smallest variation in θ_{EF} over the half-sway range. Three values of the dimensionless top-

widths, i.e. 0.23, 0.234 and 0.238 together with their dimensionless load heights gave the smallest variation in θ_{EF} over side-sway range. It is of interest to plot the change in $\dfrac{y_E}{H}$ versus dimensionless side-sway $\dfrac{x_E}{H}$ for the three dimensionless top-width values. The changes are shown in Figure 11. It is evident that, in each case, the dimensionless vertical movement of the pin joint E, where the base of the jack is connected to the GLS, is represented by a horizontal straight line over almost the whole sway-range. However, if the load-height $\dfrac{y_E}{H}$ is plotted to a finer scale, it is evident that the pin joint E exhibits very small vertical oscillations over the half-sway range and only towards the end of the sway-range does it exhibit larger reductions in $\dfrac{y_E}{H}$. Even so, converting the dimensionless values in Figure 12 to real values, it is evident that over the full $150\,mm$ sway-range, the vertical movement of the jack's pinned base at point E is less than $0.03\,mm$, which is negligible from the practical standpoint.
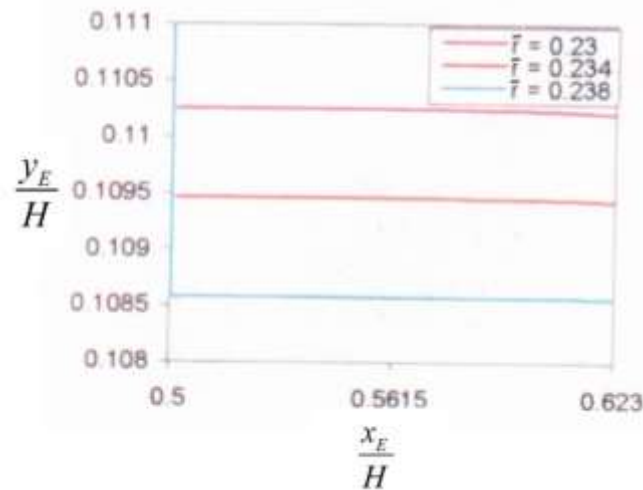

Figure 11: Coarse scale plot of vertical jack movement $\dfrac{y_E}{H}$ versus side-sway $\dfrac{x_E}{H}$
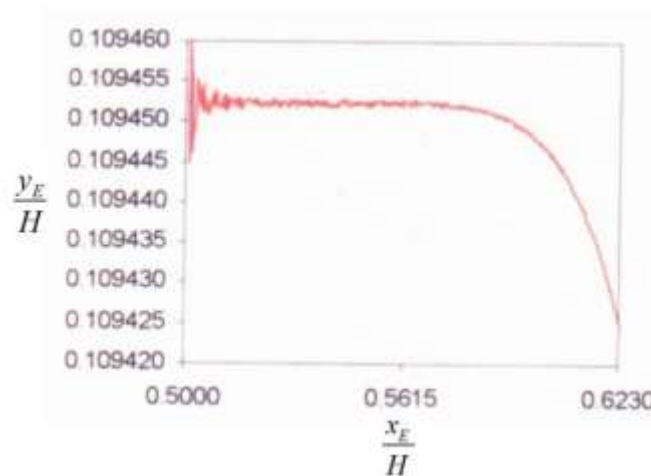

Figure 12: Fine scale plot of vertical jack movement $\dfrac{y_E}{H}$ versus side-sway $\dfrac{x_E}{H}$ ($\dfrac{r}{H} = 0.234$)

15

Having determined the geometry of the optimal GLS design, the forces may be determined in each of its members for a unit jack load applied at the pin-joint E. The graphs of these forces are shown in Figure 13 for the range of sway angles.
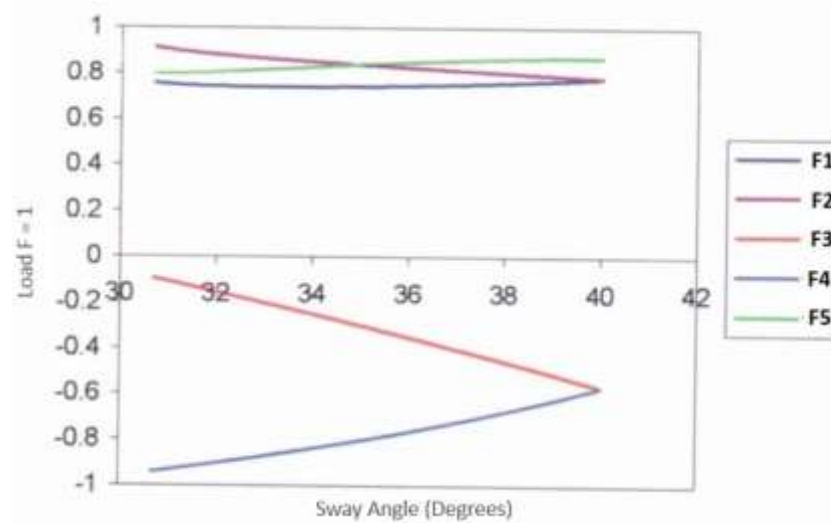

Figure 13: Member loads versus side-sway angle α (degrees) for a unit vertical load ($F = 1$) applied at the pin-joint E of the optimally designed GLS

The maximum load that the new GLS was expected to accommodate when used to investigate the lateral buckling of pultruded GFRP beams was 60 kN. Hence, from Figure 13, the maximum dimensionless load ratio for each member of the GLS was determined and then multiplied by 60 kN to give the maximum load in each member. The values of the maximum load ratios and loads are given in Table 4.

Table 4

Maximum load ratios and loads for each member of the GLS

Member	Member Length [mm]	Member Forces	Maximum Ratio of Member Forces to Unit Jack Load	Maximum Member Forces [kN]
AC	609.6	F1	0.9108	54.6
BD	609.6	F2	0.9108	54.6
CD	285.2928	F5	0.8718	52.3
CE	295.186	F3	-0.94	56.6
DE	295.186	F4	-0.94	56.6

Note: The rigid angle CED = 57.8º in Fig.8

Design and fabrication details of the GLS

In order to minimise the weight of the GLS and to ease its movement across the laboratory strong floor, it was decided to fabricate it from aluminium rather steel. This also suited the likely maximum loads that would be required when testing the lateral buckling responses of pultruded GFRP beams.

As large diameter holes were needed to accommodate the pin bearings, aluminium with an ultimate tensile strength of 280 MPa was selected, which complies with BS 5083, and is typical of that used in road, rail and shipbuilding applications. The thicknesses of the aluminium flat bar and plate were 15.875 mm).

In order to simplify the design and manufacture of members 3 – 5 (see Figure 8) they were substituted with a triangular plate. Likewise, each of the members 1 and 2 comprised of two aluminium flat plates with bearings at both ends. The central vertical member, with a large diameter hole near to its base and a smaller one at its upper end, also comprised of two aluminium flat plates, as shown in Figure 14.
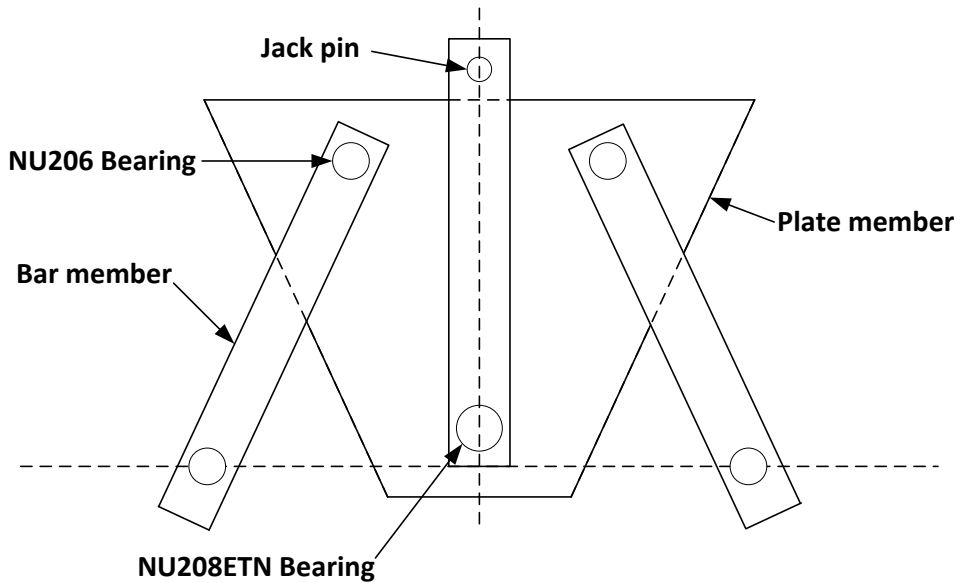
Figure 14: Schematic diagram of the members of the GLS

As each of the members 1 and 2 of the GLS comprised of two identical flat aluminium bars, they only had to support half of the load determined by the analysis (see Table 4). Thus, for the maximum design jack load of 60 kN, each of the four bars only experiences a maximum load of 27.3 kN. Hence, the pin bearings at each end of the bars must have a basic load rating greater than 27.3 kN. On the other hand, the bearing at the lower end of the vertical member (corresponding to Point E in Figure 4) must have a load bearing capacity of 60 kN.

The type of bearing used in the arrangements illustrated in Figure 14 are generally single-row radial ball bearings. However, such bearings tend to have relatively low load capacities. In order to be able to accommodate loads of 27 – 60 kN, large diameter and thickness single-row bearings are needed. Consequently, the widths or thicknesses of the aluminium bars would have to be increased, thereby increasing the overall weight of the GLS, which was unacceptable. Therefore, it was decided to use cylindrical roller bearings. Using the same diameters and thicknesses, the maximum load capacity of cylindrical roller bearings is typically 50% greater than single row radial ball bearings.

RHP bearing types NU206 and NU208ETN were selected for the GLS. NU206 bearings were used at each end of the flat bars in Figure 14 (members 1 and 2) and a NU208ETN bearing was used at the lower end of the plate member, also shown in Figure 14. Details of the geometries and load capacities of the bearing are given in Table 5 and their positions within the members 1 and 2 and the trapezoidal plate are shown in Figure 15.

Table 5

Geometries and load capacities of the NU206 and NU208ETN bearings

Bearing Type	Shaft Diameter [mm]	Hole Diameter [mm]	Thickness [mm]	Load Rating [kN]
NU206	30	62	16	33.1
NU208ETN	40	80	18	63.5

(a)
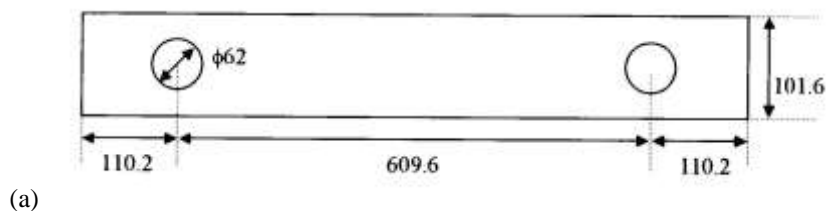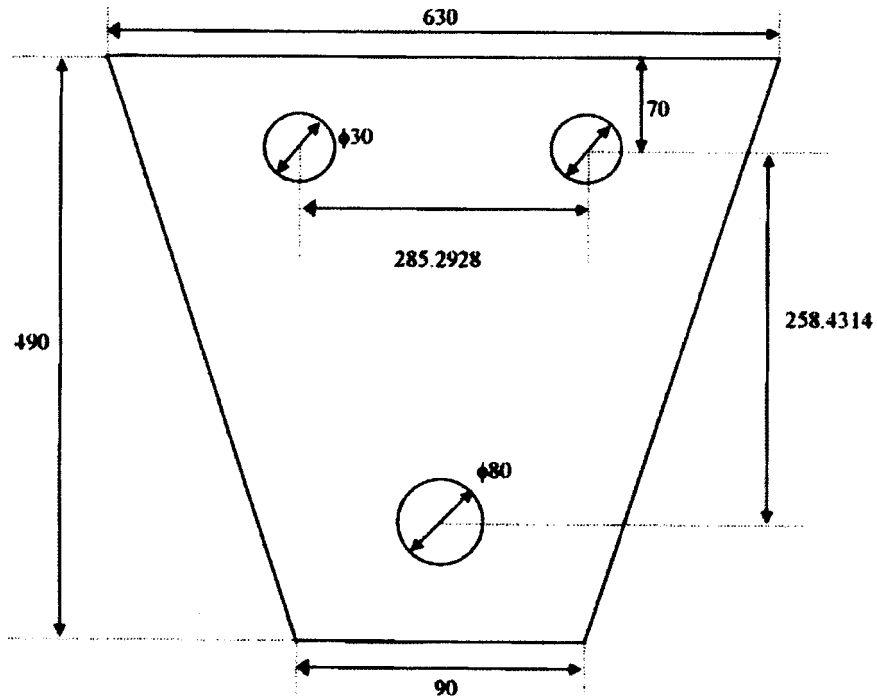
(b)

Figure 15: Schematic drawings of GLS components: (a) flat aluminium bars and (b) flat aluminium plate (dimensions in mm)

Because high stresses were expected around the holes in the flat bars and the flat triangular plate, Finite Element (FE) analyses were carried on both components for the maximum load applied to the GLS to establish that the stresses would not cause failure. Safe in the knowledge that failure of the GLS was unlikely under maximum loading, its manufacture was started and completed in about three weeks. Two images of the finished GLS are shown in Figure 16.

(a)   (b)

Figure 16: The finished GLS: (a) front view and (b) bearing connection detail

Checking the performance of the GLS

In an ideal situation, the pin joint of the GLS (see joint E of Figure 4) should move along a straight horizontal trajectory as the GLS sways to the left or right over the half-sway range. In order to check this requirement for the *as manufactured* GLS, it was set up with the two bars connected to point E (shown in Figure 16(a)) hanging downwards. An LVDT was attached to one of the bars. Due to their significant self-weight, the bars maintain

their vertical orientation throughout the sway range. Likewise, the LVDT maintains its initial vertical orientation throughout the same range. Hence, the vertical movement (y-direction) of point E is monitored.

In order to measure and record the horizontal movement (x-direction) of point E a wire-pull potentiometer (encoder) was used. One end of the string was connected to the centre of the pin joint at the top of one of the bars. The string then passed over a pulley and was kept taut by a deadweight. The test set up is shown In Figure 17.

Figure 17: Front elevation of the GLS showing the load bars downwards and the instrumentation for recording the horizontal and vertical displacement of the pin joint E as the mechanism sways

The GLS was then swayed from its initial symmetrical zero sway position to its full-sway of 150 mm, during which the vertical and horizontal (y and x) displacements were recorded. The individual vertical and horizontal displacements are shown in Figure 18(a) for the full sway range. Figure 18(a) also shows the polynomial trend line for the data points. It is evident that the vertical movement of the pin joint (point E) is less than 0.015 mm. However, if the x,y data in Figure 18(a) are plotted for the same magnitude range, then, as shown in Figure 18(b), the horizontal translation of the pin joint can be regarded as a straight line.
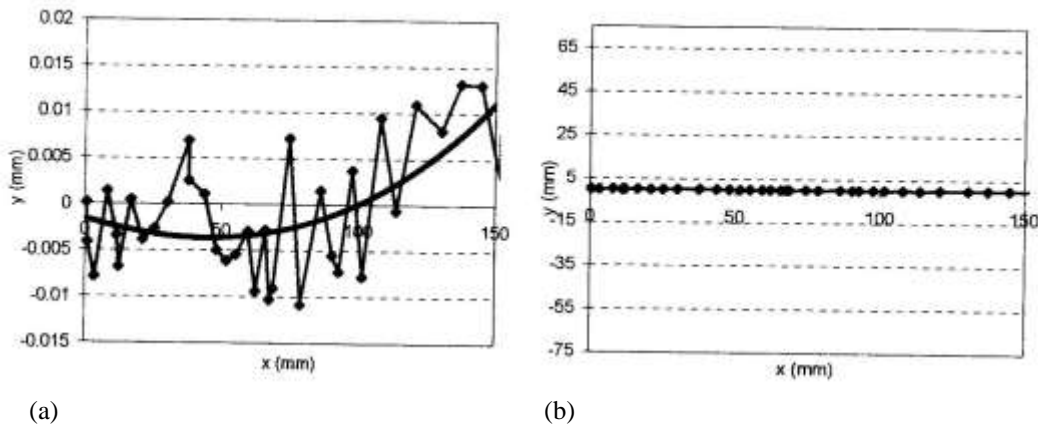

(a)   (b)

Figure 18: (a) Measured (x, y) data and polynomial trend line, (b) Normalised (x,y) data showing that the pin joint at point E effectively translates along a straight, horizontal line

The measured x and y displacements of point E, normalised to the base length H of the GLS, are also compared to the theoretically predicted values in Figure 19.
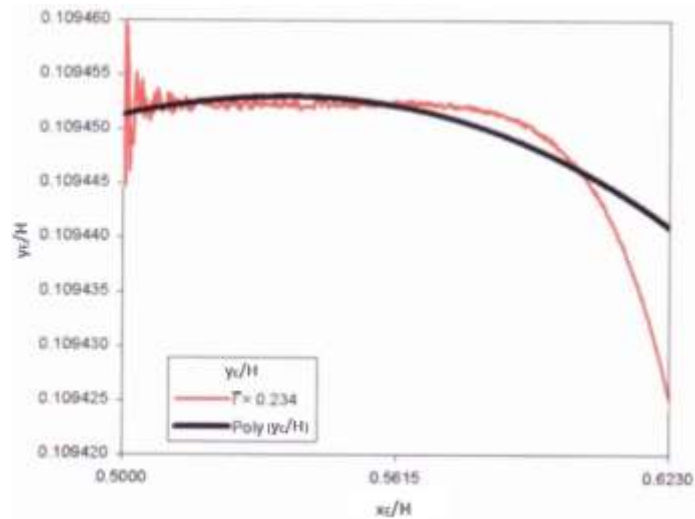
Figure 19: Comparison of the measured polynomial *best fit* $\dfrac{y_E}{H}$ versus sway displacement $\dfrac{x_E}{H}$ of the pin joint

E of the GLS mechanism

Based on the good correlation between the actual and predicted displacements shown in Figure 19, the GLS mechanism was deemed suitable for investigating the lateral buckling response of pultruded GFRP beams. An image of it in use is shown in Figure 20.
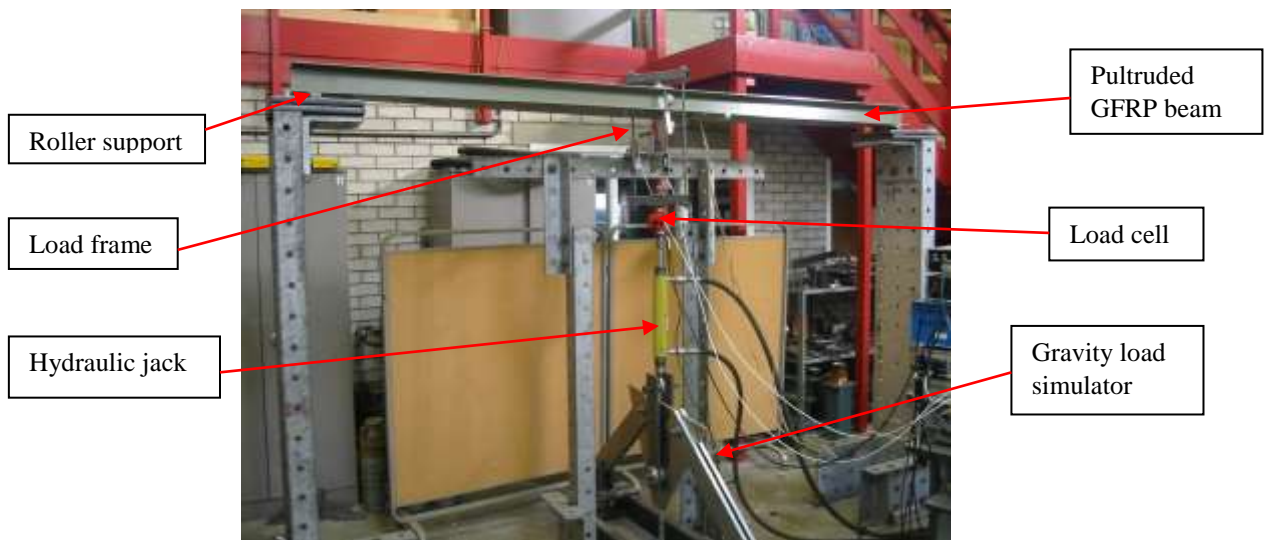

Figure 20: Image of the aluminium GLS mechanism used to conduct a lateral bucking tests on a simply supported pultruded GFRP WF beam

Concluding Remarks

Details of the exact analysis, design, manufacture and test verification of an aluminium GLS are presented. GLS's are used in beam and/or frame lateral buckling tests to overcome lateral restraint due to fixed base jack loading.

The exact GLS analysis is simpler to use than Yarimci et al's [14] iterative analysis and, moreover, is more accurate.

The exact analysis was used to develop an optimised GLS design. The load analysis of the GLS has enabled its member sizes and joint types/capacities to be determined.

The designed GLS was manufactured using aluminium bar and plate and two types cylindrical roller bearings. Its performance was verified by conducting tests to measure the vertical and horizontal displacements of the pin joint E over the full-sway range. These tests confirmed the accuracy of the GLS for lateral buckling tests on pultruded GFRP beams.

Acknowledgements

References

1. Anon., Load and Resistance Factor Pre-Standard for Pultruded for Pultruded GFRP Structures, *American Composites Manufacturers Association*, 2012.

2. Ascione L, et al. (Eds), Prospect for New Guidance in the Design of FRP Structures, *European Composites Industry Association (EuCIA)*, Brussels, 2016.

3. Mottram JT, Henderson J (Eds), FRP Bridges – Guidance for Design, Report C779, *Construction Industry Report and Information Association (CIRIA)*, London, 2018.

4. Mottram JT, Structural properties of a pultruded E-glass fibre-reinforced I-beam, *Proceedings of the 6th International Conference on Composite Structures*, Elsevier Applied Science, London, 1991, 1-28.

5. Mottram JT, Lateral-torsional buckling of a pultruded I-beam, *Composites*, 23(2) 1992, 81-93.

6. Turvey GJ, Lateral buckling tests on rectangular cross-section pultruded GRP cantilever beams, *Composites Part B*, 27B(1), 1996, 35-42.

7. Turvey GJ, Effect of load position on the lateral buckling response of pultruded GRP cantilevers – Comparison between theory and experiment, *Composite Structures*, 35(1), 1996, 33-47.

8. Qiao PZ, Zou GP, Davalos JF, Experimental and analytical evaluation f lateral bucking of FRP composite cantilever I-beams, *Proceedings of the 3rd International Conference on Composites in Infrastructure (ICCI'02)*(CD ROM), 2002, Paper 017, pp.11.

9. Qiao PZ, Zou GP, Davalos JF, Flexural-torsional buckling of fiber-reinforced plastic composite cantilever I-beams, *Composite Structures*, 60(2) 2003, 205-217.

10. Shan LY, Qiao PZ, Flexural-torsional buckling of fiber-reinforced plastic composite open channel beams, *Composite Structures*, 68(2), 205, 211-224.

11. Nunes F, Correia JR, Silvestre N, Structural behaviour of hybrid FRP pultruded beams: Experimental, numerical and analytical studies, *Thin-Walled Structures*, 106, 2016, 201-217.

12. Nguyen TT, Chan TM, Mottram JT, Experimental determination of the resistance of pultruded FRP beams failing by lateral torsional buckling, *Proceedings of the 6th International Conference on Advanced Composites in Construction*, Net Composites Ltd, Chesterfield, UK, 2013, 252-263.

13. Nguyen TT, Chan TM, Mottram JT, Lateral-torsional buckling resistance by testing of pultruded FRP beams under different loading and displacement boundary conditions, *Composites Part B: Engneering*, 60(1), 2014, 233-242.

14. Yarimci E, Yura JA, Lu LW (1967), Techniques for testing structures permitted to sway, *Experimental Mechanics*, 7(8), 321-331.